Electronics Irradiation With Neutrons at the NEAR Station of the n_TOF Spallation Source at CERN

Matteo Cecchetto, Mario Sacristan Barbero, *Member, IEEE*, Giuseppe Lerner, Rubén García Alía, *Member, IEEE*, Ygor Aguiar, *Member, IEEE*, Dominika Senajova, Francisco Garcia Infantes, Jose Antonio Pavon Rodriguez, Marta Sabate Gilarte, Vasilis Vlachoudis, Ana-Paula Bernardes, Marco Calviani, and Salvatore Danzeca, for the n_TOF Collaboration

***Abstract*— We study the neutron field at the NEAR station of the neutron time-of-flight (n_TOF) facility at CERN, through Monte Carlo simulations, well-characterized static random access memories (SRAMs), and radio-photoluminescence (RPL) dosimeters, with the aim of providing neutrons for electronics irradiation. Particle fluxes and typical quantities relevant for electronics testing were simulated for several test positions at NEAR and compared to those at the CERN high-energy accelerator mixed-field facility (CHARM), highlighting similitudes and differences. The SRAM detectors, based on single-event upset (SEU) and single-event latch-up (SEL) counts, each one with a different energy response, and RPL dosimeters were tested in a reference position, and the results were benchmarked to FLUKA simulations. Finally, the neutron spectra at NEAR are compared to those of the most well-known spallation sources and typical environments of interest, for accelerator and atmospheric applications, showing the potential of the facility for electronics irradiation.**

***Index Terms*— CERN high-energy accelerator mixed-field facility (CHARM), FLUKA Monte Carlo simulations, NEAR, neutron time-of-flight (n_TOF), neutrons, radio-photoluminescence (RPL), single-event effects (SEEs), spallation facilities, static random access memory (SRAM).**

I. Introduction

NEUTRONS are among the major contributors to single-event effects (SEEs) in electronic devices, as far as accelerator and atmospheric applications are concerned. These environments are characterized by neutron spectra ranging several orders of magnitude, with energies from meV (thermal) up to a few GeV in the accelerator context and as high as 100 GeV in the atmosphere. Electronic components that need to operate in such environments are preventively tested in dedicated facilities with the aim of reproducing as well as possible the operational conditions. Several sources can be employed for the neutron SEE qualification of electronics. A spallation neutron source provides the closest shape to the atmospheric spectrum, as stated in the JEDEC JESD89A standard [1] for ground-level applications and in the IEC 62396-1 [2] and IEC 62396-2 standards [3] for avionics. Some of the most well-known neutron spallation facilities are WNR-Los Alamos Neutron Science Center (LANSCE), Los Alamos, NM, USA, TRIUMF, Vancouver, CA, USA, Research Center for Nuclear Physics (RCNP), Osaka, Japan, ChipIr, Didcot, U.K. In addition, the CSNS facility was recently built, in China, while ANITA, Uppsala, Sweden, is no longer in use. Regarding accelerator environments, specifically for the large hadron collider (LHC) accelerator at CERN, both neutron spallation sources and mixed-field facilities can be employed depending on the properties to mimic (energy spectra, type of particles, etc.) [4]. In this regard, the CERN high-energy accelerator mixed-field facility (CHARM) [5] was compared in [4] to the ChipIr [6] facility, which is currently the reference spallation facility in Europe for electronics irradiation.

However, the increasing demand for accelerated testing of electronic components needed to operate in accelerator and atmospheric environments has led to the investigation of the potential employment of the neutron time-of-flight (n_TOF) spallation facility at CERN [7], which is normally used for very accurate neutron reaction cross section measurements.

In this work, we study through Monte Carlo simulations and well-calibrated static random access memory (SRAM) measurements whether the neutron field at the NEAR station, which is a recently built area at the n_TOF facility, can be employed for SEE electronics testing for accelerator and atmospheric applications. A comprehensive analysis to fully characterize the NEAR station was performed through FLUKA simulations [8], [9], [10], where ten hypothetical test positions were identified and the typical quantities used for irradiation of electronics were calculated. Regarding the measurements, as the spectrum to be characterized ranges over several orders of magnitude, the approach we employed consists of combining several SRAM detectors, which have shown to be sensitive to different portions of the spectrum in previous publications [4], [11]. The measurements were compared to FLUKA Monte Carlo simulations for one reference position to validate the approach. Other techniques could be employed to measure the neutron spectra, for instance, through a Bonner sphere or activation foils, but they were not explored in this work. Moreover, dose measurements by means of radio-photoluminescence (RPL) detectors [12] and dose simulations were performed to quantify the photon fluence

Manuscript received 24 December 2022; revised 19 January 2023; accepted 30 January 2023. Date of publication 3 February 2023; date of current version 16 August 2023.

The authors are with CERN, 1211 Geneva, Switzerland.

Color versions of one or more figures in this article are available at https://doi.org/10.1109/TNS.2023.3242460.

Digital Object Identifier 10.1109/TNS.2023.3242460

and assess whether the facility could be employed to perform also cumulative effects testing.

In addition, the fluxes and spectra at the NEAR station were compared to those of other spallation facilities, locations in the LHC, the ground-level and avionic environments, and test positions at CHARM, currently, the mixed-field facility employed for electronics qualification at CERN. As it will be shown, one of the main differences between NEAR and CHARM relies on the particle composition of the respective spectra.

II. NEAR Station at the n_TOF Facility

n_TOF is one of the few spallation facilities in the world that provides neutron spectra, which are employed in two experimental areas (EAR1 [13] and EAR2 [14]) for very accurate cross section measurements via the time-of-flight technique. The facility has been operating since 2001 [15] and has been providing a rich scientific program for astrophysics, nuclear technologies, and medical applications [16]. Neutrons at n_TOF are produced by the interaction of a 20-GeV pulsed proton beam at high intensity, extracted from the proton synchrotron (PS), with a pure lead target cooled down with gaseous nitrogen. Each pulse delivers an average of 7×10^{12} protons [13] in only 6 ns, and the time structure consists of a cycle composed of six pulses separated by 1.2 s plus 30 s of cool-down time [17], [18]. During 2022, the average protons on target (POT) delivered to n_TOF were 3.9×10^{15} POT/h, while the same value delivered to CHARM, which is also fed by the PS, was 1.1×10^{14} POT/h. Hence, 35 times more POT were injected at n_TOF with respect to CHARM.

Following the upgrades carried out in 2021, the NEAR station, a third irradiation area, has been constructed in the proximity of the n_TOF target and can be subdivided into two main regions. The location inside the shielding of the target has the aim of providing high dose levels (on the order of MGy) to study radiation damage in materials [19], while the location outside the shielding was employed in this work for electronics irradiation. Specifically, the shielding incorporates a collimator so that a portion of the produced high-intensity neutrons can be conveyed in the outside area, as detailed in [19]. Several test positions were characterized through simulations for electronics irradiation (see Section IV-A), and the test position on a plane perpendicular to the collimator at about 2.5 m from it (5 m from the center of the target), as shown in Fig. 1, was also calibrated with measurements. The access and beam time at NEAR are regulated according to the n_TOF schedule, with access time varying along the year and usually taking place every two to four weeks when the beam is stopped for a few days. Hence, the irradiation time and access for the installation/replacement of electronic devices depend on the physics program of the experimental areas. As the NEAR station is close to the target, the time allowed to personnel for the installation is very limited due to radiation protection constraints.

III. SRAM and RPL Detectors

To measure and characterize the wide energy spectrum at NEAR, as described in [4], four types of commercial

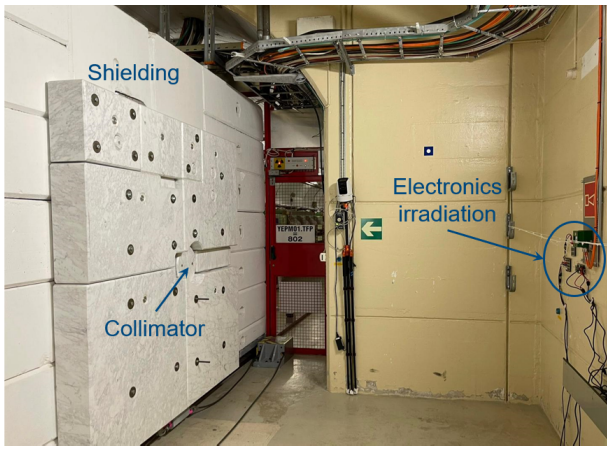

Fig. 1. Photograph of the NEAR station for irradiation of electronics. On the left, the concrete and marble shielding, beyond which the lead target is installed and, on the right, the position on the wall, perpendicular to the collimator, characterized through Monte Carlo simulations, electronic devices, and RPL dosimeters.

TABLE I
Specifications of SEU and SEL SRAM Detectors Employed for This Work

Memory	Reference	Date code	Tech. [nm]	Size [Mbit]
ISSI (SEU)	IS61WV204816BLL-10TLI	1650	40	32
Cypress (SEU)	CY62167GE30-45ZXI	1731	65	16
Alliance (SEL)	AS7C34098A-10TCN	1339	200	4
Samsung (SEL)	K6R4016V1D-TC10	413	180	4

off-the-shelf (COTS) SRAMs were employed [recording single-event upsets (SEUs) and single-event latch-ups (SELs)] as reported in Table I, whose response functions were well-characterized in several facilities [11], [20]. The response of the SRAMs as a function of the neutron energy is shown in Fig. 2, considering the absolute values of the SEE cross sections to better visualize their differences. The curves above 0.01 meV are reported from [11] and [20], [21] with regard to the SEU and SEL SRAMs, respectively, and were calculated by fitting the experimental SEE cross sections measured with monoenergetic neutrons (for SEU) or protons (for SEL) with a Weibull function. SRAMs of the same type were employed in several other works, with applications ranging from SEE studies and predictions in the accelerator, atmospheric and space environments [11], [20], [21], [22], [23], [24] to facility, and radiation fields characterization [4], [25].

The SEU and SEL response function of SRAMs is described as follows.

1) *SEU-Sensitive SRAMs:* The thermal neutron equivalent (ThNeq) and high-energy hadron equivalent (HEHeq) fluences are used to describe the SEU response through the following equation:

$$\Phi_{\text{ThNeq}} = \int_0^{+\infty} \sqrt{\frac{0.025\ \text{eV}}{E[\text{eV}]}} \cdot \frac{d\Phi_n(E)}{dE}\, dE. \quad (1)$$

$$\Phi_{\text{HEHeq}}^{\text{SEU}} = \int_{E_{\text{th}}}^{20} w_A(E) \cdot \frac{d\Phi_n(E)}{dE}\, dE + \int_{20}^{+\infty} \frac{d\Phi_{\text{HEH}}(E)}{dE}\, dE. \quad (2)$$

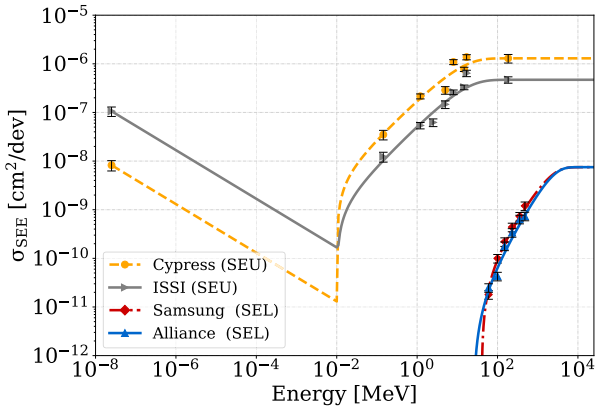

Fig. 2. Response function of the SRAM devices as a function of the neutron energy, as described by (1) and (2) for SEUs and (3) for SELs. In addition, the experimental SEE cross sections are shown with the associated error bars.

In the Φ_{ThNeq} definition, the neutron fluence ($\Phi_n(E)$) is weighted with a function, which has a value of unity at 25 meV, and decreases as a function of the neutron velocity. Φ_{HEHeq} is defined in the accelerator context as the fluence of intermediate energy neutrons between an energy threshold E_{th} and 20 meV, which is memory-dependent through a Weibull function $w_A(E)$, plus the fluence of hadrons (neutrons, protons, pions, kaons) above 20 meV (Φ_{HEH}) [26]. The cutoff at 20 meV is based on the fact that charged hadrons with lower energy will not pass through the chip package or they will not be able to induce inelastic interactions, which release most of the charge to trigger SEUs [27]. Note that, as will be shown in Section IV, the HEH term can be considered as composed of only neutrons at NEAR, but the HEH notation is kept for compatibility with other previous publications and comparison to other environments.

The ISSI 40-nm memory has a high thermal neutron SEU cross section, which is only three times lower than the high-energy hadron (HEH) one [23], while the Cypress 65-nm memory is almost nonsensitive to thermal neutrons (the aforementioned ratio is larger than 100) [11]. Both memories instead present a relatively high SEU cross section to intermediate energy neutrons between 0.1 and 10 meV. The thermal neutron (25 meV) SEU cross sections in Fig. 2 were measured in a nuclear reactor ([23], [28]) and the $1/v$ fitting until 0.01 meV is determined according to (1).

2) *SEL-Sensitive SRAMs:* Unlike those for SEUs, these memories are sensitive to hadrons with energies generally above the threshold of ∼20 meV, as described in the following equation:

$$\Phi^{\text{SEL}}_{\text{HEHeq}} = \int_{E_{\text{th}}}^{+\infty} w_B(E) \cdot \frac{d\Phi_{\text{HEH}}(E)}{dE}\, dE. \tag{3}$$

Their response function is normally less energy-dependent than that of SEUs, hence, the Weibull function $w_B(E)$ is often approximated to be unitary. However, for the specific case of Alliance and Samsung memories employed in this work, their SEL cross section does not saturate at 200 meV but only after a few GeV, and their response was characterized in dedicated studies [22], [29]. For this peculiarity, they are employed to extract information about the hardness of a spectrum.

The number of SEEs in SRAMs is calculated according to the following equation:

$$N_{\text{SEE}} = \sigma_{\text{HEH}} \cdot \Phi_{\text{HEHeq}} + \sigma_{\text{ThN}} \cdot \Phi_{\text{ThNeq}}. \tag{4}$$

Here, σ_{ThN} and σ_{HEH} are the thermal neutron and HEH saturated cross sections at high energy, respectively, and Φ_{HEHeq} is different for each memory, as it depends on the SEE response function according to (2) and (3). It is noteworthy that, for the SEL-sensitive SRAMs, the thermal neutron part is absent, as the energy and LET of the related products are not sufficient to induce latch-ups.

The four SRAM devices were installed on the wall in front of the collimator (see Fig. 1), at 10 cm of distance from the projection of its center: on the top (Samsung), left (Alliance), bottom (Cypress), and right (ISSI) positions (see also Fig. 11, which will be explained in Section V). The SEU detectors were composed of a single SRAM installed in a readout motherboard housing a ProAsic 3 FPGA, which permits reading/writing the memory and communicating with a laptop through USB protocol, the latter extended with a USB to the Ethernet connection. No shielding was installed on the motherboard to protect against radiation and the power of 3.3 and 5 V was carried via BNC cables. The SEL detectors consisted of a motherboard housing eight SRAMs of the same reference, to increase the statistics because of their lower sensitivity. All the SRAMs were powered at 3.3 V and controlled with dedicated software from a laptop, at about 70 m from the irradiation room, and this was one of the main constraints concerning signal communication for the SEU tester. The irradiation took place for a period of about 15 and 30 days for the SEU and SEL boards, respectively, and a detailed analysis of the particle fluxes is presented in Section IV.

In addition, RPL dosimeters were employed to measure the dose on the same positions of the SRAMs during a second run. These dosimeters are very compact passive monitors that can measure doses in the range of 1 Gy to ∼2 MGy [12].

IV. Fluxes and Radiation Field Analysis Through Monte Carlo Simulations

The FLUKA Monte Carlo code was used to simulate the particle fluxes relevant to the irradiation of electronics in the whole NEAR station outside the shielding; compare them to those at CHARM and benchmark the SRAM measurements.

A. NEAR FLUKA Simulations

Ten test positions, identified outside the shielding (NEAR-out) subject of the study, are shown in Fig. 3, of which N1–N4 in front of the collimator are the main test positions, while N5–N10 perpendicular to the collimator's axis are included for completeness. Each test position is considered

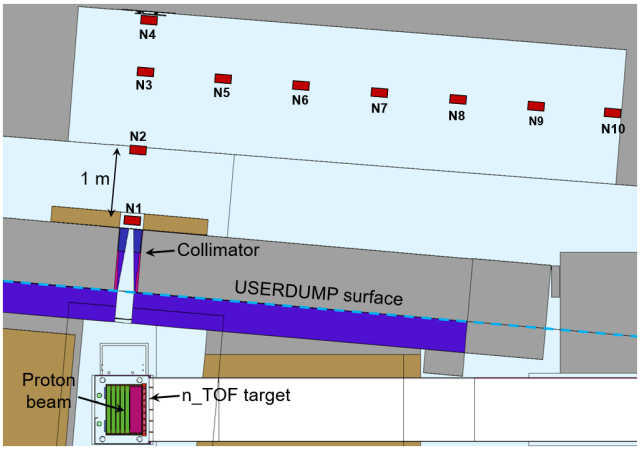

Fig. 3. Top view of the NEAR geometry in FLUKA with ten test positions (N1–N10) analyzed in this work, of which N1–N4 are of major interest because they are situated in front of the collimator. The n_TOF lead target and the direction of the incoming proton beam from the PS are shown at the bottom. The dashed line refers to the USERDUMP surface employed for the second step simulation, set between the iron (blue) and concrete (gray) shielding.

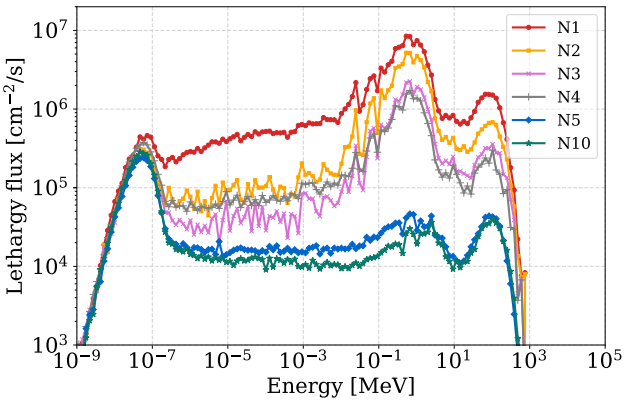

Fig. 4. Lethargic neutron spectra at NEAR of several test positions simulated with FLUKA: N1–N4 are in front of the collimator, while N5 and N10 are outside the main beam. The spectra are normalized per second considering the average POT delivered to n_TOF in 2022, which corresponds to 3.9×10^{15} POT/h.

as a cylinder with both a radius and length of 10 cm, located at a height of 120 cm from the floor, with a spacing of 1 m among each other (except for N4 which is at 66 cm from N3). N1 is right outside the collimator (∼2 m from the target) and N4, of particular interest because the SRAM measurements took place here, is located very close to the wall (∼5 m from the target).

Given the complexity of the n_TOF FLUKA geometry, where particles have to be generated from the interaction proton–target and travel several meters through the thick shielding until arriving at a test position, to obtain proper statistics in a reasonable time, a two-step simulation approach was adopted. In the first phase, the transport of a particle produced in the target is performed until crossing the surface shown in the dashed line in Fig. 3, between the iron (blue) and concrete (gray) shielding. On this surface, the properties of a particle (type, position, direction, and energy) are saved using the USERDUMP card in FLUKA [30]. Second, the previous information is used as an input for the second step simulation, in which the particle transport starts from the aforementioned surface (hence, there is no need to simulate again the proton–target interactions, which take a considerable amount of time).

Fig. 4 shows the simulated neutron spectra for the significant test positions in front of the collimator (N1–N4) and on the side (N5 and N10), while N6–N9 were omitted as their spectra are very similar to that of N10. The y-axis is represented in lethargy, which is defined as the product of the differential flux by the geometric mean of the corresponding energy bin. As a result, the area under the lethargy curve between two energies is proportional to its integral flux, although both the x and y scales are logarithmic. As can be expected, the positions in front of the collimator present the larger fluxes but all spectra range from the thermal component (peak around 25 meV) up to ∼830 meV, and with well visible evaporation (∼1 meV) and spallation (∼100 meV) peaks. In spallation reactions, where protons typically impact against a heavy-Z target, other particles in addition to neutrons are produced, such as secondary hadrons (protons, pions, and kaons). However, the flux of these secondary particles was shown to yield a negligible contribution (<0.3%), and hence the radiation field can be considered as composed of only neutrons. Even considering the electromagnetic (EM) component (dominated by photons) in the percentage, the radiation field throughout the NEAR station is composed of at least 80% of neutrons.

B. NEAR Fluxes–CHARM Comparison

Spectra, fluxes, and the typical quantities used for electronic irradiations were calculated at NEAR and compared to those obtained in test positions at CHARM [5], currently the mixed-field facility employed for electronics qualification at CERN.

Fig. 5 depicts the top view of the CHARM facility, showing the direction of the incoming 24-GeV proton beam impinging a target and the four blocks of movable concrete (C) or iron (I) shielding, whose aim is to modulate the radiation field in the lateral positions (R1–R10). Different targets and shielding can be used, but in the following analysis, the copper target with no shielding (CUOOOO) and full shielding (CUCIIC) will be considered, where the former is the typically used configuration as it enables the production of the highest dose and HEH flux values, while the latter permits to produce the larger neutron fluxes.

Among the more than 13 test positions at CHARM, four are included in the comparison, in the following sorted with increasing hardness of the spectrum: G0 on the corridor outside the main irradiation chamber presents the softer spectrum, R1, R10 (hard spectrum), and R13, almost perpendicular to the direction of the incoming proton beam impacting the target. Although R12 would show a larger flux of particles with high energies, it is hardly used in practice due to its poor homogeneity, and hence, R13 is preferred.

The NEAR and CHARM spectra are shown in lethargic units in Fig. 6, and in differential units above 1 meV in Fig. 7 to better illustrate the differences at high energies. In terms

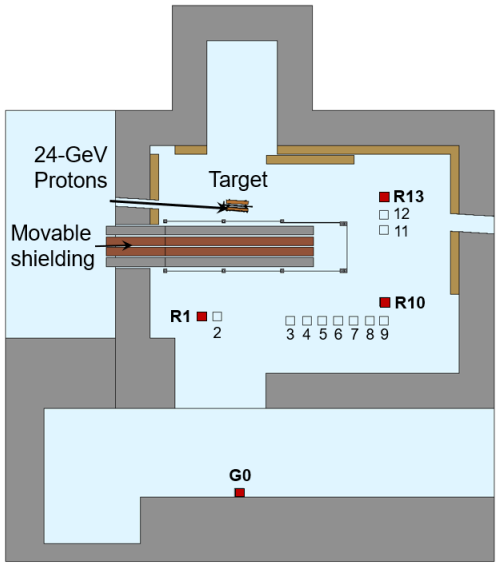

Fig. 5. Top view of the CHARM facility, showing the 13 main test positions (R1–R13) inside the irradiation chamber in addition to G0 in the corridor. R1, R10, R13, and G0, highlighted in red, are the subject of the analysis in this work.

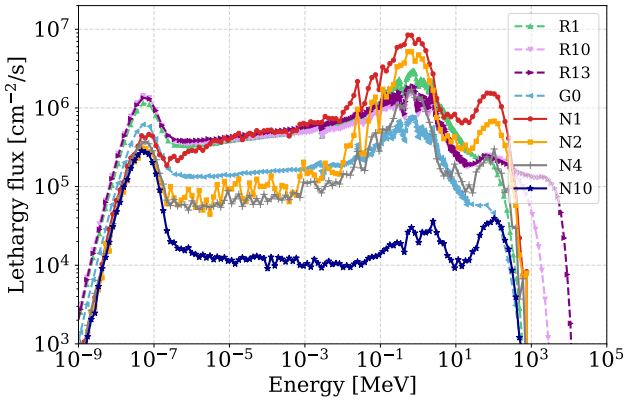

Fig. 6. Lethargic neutron spectra of significant test positions at NEAR (N1, N2, N4, and N10) and CHARM (R1, R10, R13, and G0), configured with copper target and no shielding. The spectra are normalized per second considering the average POT delivered to n_TOF and CHARM in 2022, which corresponds to 3.9×10^{15} and 1.1×10^{14} POT/h, respectively.

of maximum neutron energy, N1–N4 (∼830 meV) are very similar to R1 (∼960 meV), while R10 and R13 reach up to 5 and 12 GeV, respectively. Moreover, N4 and R1 show very similar spectra shape above 60 meV, while below this energy, R1 has higher fluxes than N4 (see Fig. 7). N1 and N2 present instead the larger fluxes between 30 and 200 meV, and as a general fact, the spectra at NEAR have a thermal neutron peak several factors lower than the spectra at CHARM (see Fig. 6).

In addition, the HEH flux considers particles above 20 meV, which are neutrons at NEAR but includes also protons and pions at CHARM (due to the mixed-field). Indeed, although both n_TOF and CHARM radiation fields are generated by the interaction of a high-energy proton beam with a target (of lead and copper, respectively), the particle composition is very different. This has to be attributed to the dimension of the targets, which is smaller at CHARM (50-cm long, 8-cm

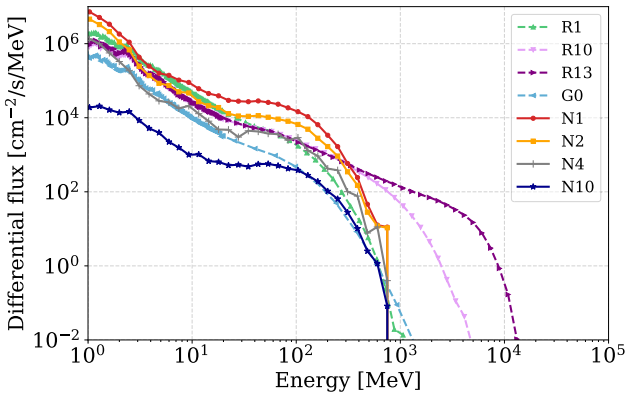

Fig. 7. Differential neutron spectra above 1 meV of significant test positions at NEAR (N1, N2, N4, and N10) and CHARM (R1, R10, R13, and G0), configured with copper target and no shielding. The spectra are normalized per second considering the average POT delivered to n_TOF and CHARM in 2022, which corresponds to 3.9×10^{15} and 1.1×10^{14} POT/h, respectively.

diameter) compared to that at n_TOF (63-cm long, surface of 70×76 cm^2). Hence, the major difference is in the radial thickness of the targets and material density, which play as a filter for charged particles. The production and transport of EM and hadronic showers are illustrated in the simplified simulations of Fig. 8, considering a 24-GeV proton beam on a copper target ($\rho = 8.96$ g/cm^3) for CHARM and a 20-GeV proton beam on a lead target ($\rho = 11.35$ g/cm^3) for NEAR, both in vacuum to emphasize secondaries from the targets. In n_TOF, protons, pions, and the EM component produced around the center of the target along the proton beam direction will be mostly shielded by its thickness and density, resulting in stronger neutron domination in output, while at CHARM, the smaller radial thickness and density of the target will permit charged hadrons and EM showers to escape and contribute with neutrons to the mixed-field.

Fig. 9 reports the simulated fluxes and dose at NEAR and CHARM (the latter with no shielding to obtain the larger fluxes), normalized per hour for a direct comparison, considering the POT delivered in 2022 as mentioned in Section II. For comparison, the HEH yearly fluence in some locations in the LHC can reach up to 10^{11} HEH/year [31]. Neutrons and thermal neutrons (ThNeq) are the fluxes of total neutrons by integrating the full spectra of Fig. 6 and by applying (1), respectively. Finally, the equivalent flux of 1-meV neutrons (1 meV-neq) that are representative of displacement damage (DD) effects and the dose is displayed in Fig. 9. From these results, several observations can be drawn and are listed below.

1) Dose levels are generally lower at NEAR; hence, the HEH/dose ratio is larger, which is suitable for SEE testing.
2) N1 shows the highest neutron flux with respect to all the 13 positions at CHARM, and comparable HEH flux as in R13, while N2 and N4 have similar HEH fluxes to R10 and R1, respectively.
3) Focusing on N4, its HEH flux has the same order of magnitude as that in R1 at CHARM (see Figs. 7 and 9). Moreover, the 1-meV-neq flux is larger in R1 than in N4. These observations show that the flux in N4 at high

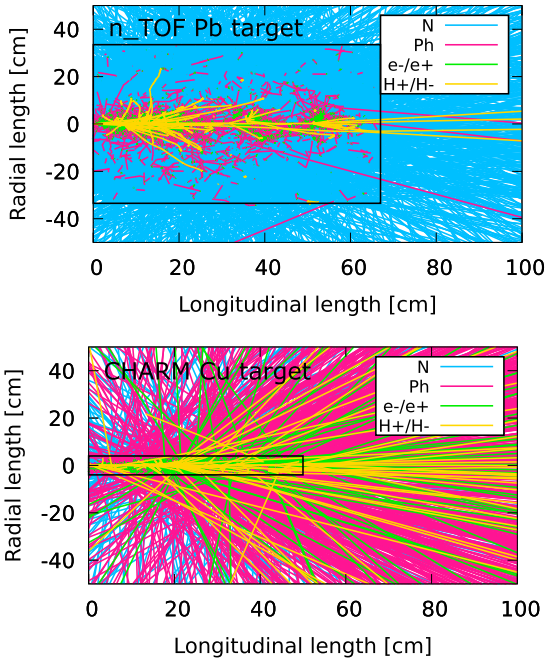

Fig. 8. Production of neutrons (N), photons (Ph), electrons/positrons (e−/e+), and charged hadrons (H+/H−) in the n_TOF (top picture) and CHARM (bottom picture) targets. The proton beam is coming from the left at (0,0) coordinates, considering only five primaries to limit the number of secondaries which otherwise would saturate the plot.

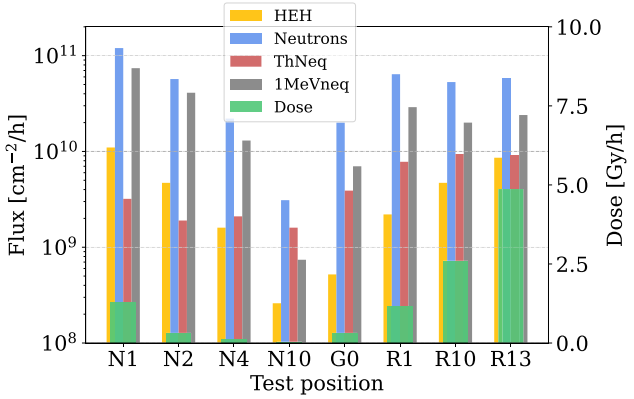

Fig. 9. Simulated fluxes of HEH, neutrons, ThNeq, 1 meV-neq (left axis), and dose (right axis) for several test positions at NEAR (N1, N2, N4, and N10) and CHARM (G0, R1, R10, and R13), the latter configured with a copper target and no shielding (CUOOOO). The results are normalized per hour for a direct comparison.

energies (∼100 meV) is similar to that in R1, but at lower energies, the neutron flux at CHARM is larger than that in N4.

4) The positions N5–N10 at NEAR, which are outside the collimator's axis, present very similar fluxes. However, the HEH values are about one order of magnitude lower compared to those in front of the collimator, but the homogeneity is very good along several meters. Hence, this area could be used for system-level testing, even with equipment of large dimensions, as they typically require lower fluxes than single components.

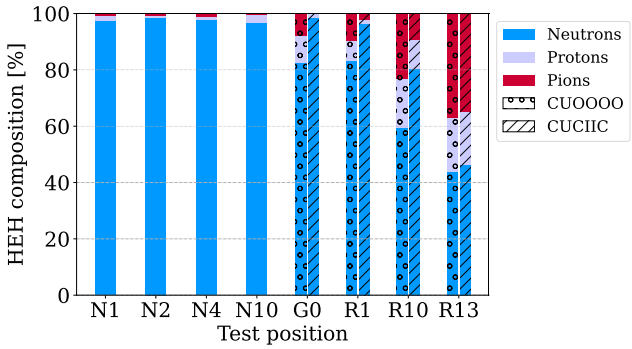

Fig. 10. HEH (>20 meV) particle composition (neutrons, protons, and pions) expressed in percentage for several test positions at NEAR (N1, N2, N4, and N10) and CHARM (G0, R1, R10, and R13), the latter configured with a copper target and no shielding (CUOOOO) and full shielding (CUCIIC).

The HEH flux is an important figure, especially for SEU testing, as the SEU cross section of electronic devices is typically in saturation above 20 meV. As mentioned in Section III, the HEH flux, defined as composed of hadrons above 20 meV, is mainly given by the contribution of neutrons, protons, and pions, whose percentages are depicted in Fig. 10 for the several positions at NEAR and CHARM. Although these particles are often assumed to be equally effective in inducing SEEs, this is not always the case, especially for pions, which can exhibit a different SEE cross section at high energies [32]. Hence, depending on the environment of interest and the test requirements of electronics, a pure neutron spectrum can be preferable for the test.

As can be seen in Fig. 10, more than 97% of the HEH flux at NEAR is composed of neutrons, while the neutron percentage at CHARM without shielding is lower, ranging from a maximum of 84% in G0 to a minimum of 44% in R13, where protons and pions yield instead the dominant contribution. The neutron contribution at CHARM can be increased up to 98% only on the lateral positions when introducing the full shielding.

V. Characterization of N4 Through Measurements and Simulations

The position on the axis of the collimator situated on the wall (N4) is studied in more detail, as it was characterized also with SRAM and RPL measurements, to benchmark the simulations and to validate the neutron fluence and dose values.

A. SRAM Measurements and Benchmark With Simulations

As the neutron field is directed to the SRAMs through the collimator, its homogeneity is assessed through simulations to ensure the correctness of the measurements, and the HEH flux is shown in Fig. 11. The SRAM positions and their E_{th} are shown on the top of the graph in the same figure and the corresponding homogeneity is within 30%. In addition, the plot gives an estimation of the maximum dimensions of a possible electronic board/system that can be tested at the center of this location with a certain homogeneity, for

TABLE II

SIMULATED NEUTRON FLUX AT THE POSITION OF THE ALLIANCE MEMORY, CONSIDERING THE AVERAGE POT DELIVERED DURING THE MEASUREMENTS (2.8×10^{15} POT/h)

Flux	ThNeq	> 10MeV	> 20MeV	Total
[n/cm^2/s]	6.4×10^5	4.2×10^5	3.5×10^5	5.9×10^6

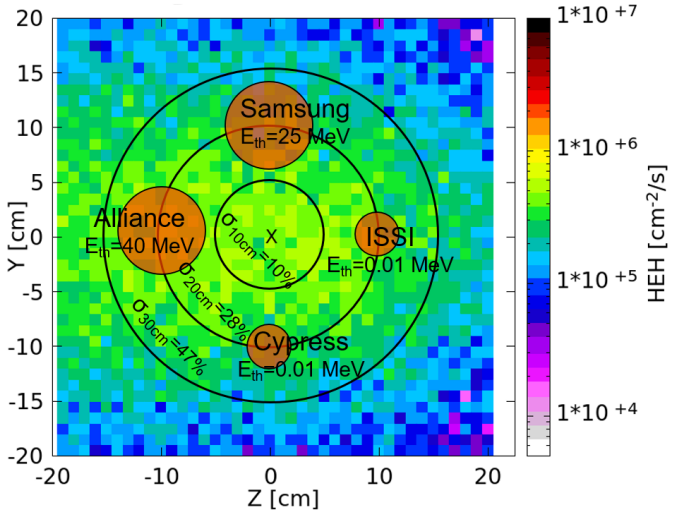

Fig. 11. Homogeneity map on the position of the SRAMs showing the HEH (>20 meV) flux simulated with FLUKA. The SRAM positions are shown on the top of the graph, reporting also their energy threshold (E_{th}) used in (2) to calculate the HEHeq fluence.

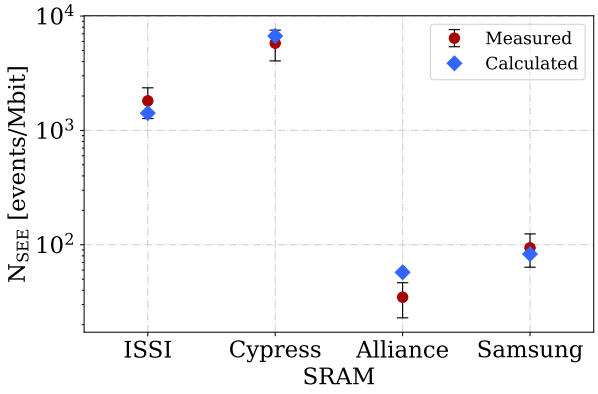

Fig. 12. SEE counts measured by the SRAMs (SEUs for ISSI and Cypress, SELs for Alliance and Samsung), normalized to the size (Mbit) of each memory, in comparison to the events calculated through (4) using the simulated NEAR spectrum in N4. SEEs measured during irradiation with 1.2×10^{17} POT lasted 43 h.

TABLE III

MEASURED AND SIMULATED DOSE AT THE POSITION OF THE SRAMS ON THE WALL (THE RPL'S NOMENCLATURE IS BASED ON THE INITIAL LETTER OF THE SRAM TO IDENTIFY ITS POSITION) AND ON THE CENTER OF THE PROJECTION OF THE COLLIMATOR. THE PERCENTAGE REFERS TO THE DIFFERENCE BETWEEN THE MEASURED DOSE WITH RESPECT TO THE SIMULATED VALUE. THE DOSE LEVELS REFER TO 8.4×10^{18} POT

	RPL-0	RPL-A	RPL-I	RPL-S	RPL-C
Sim. Dose [Gy]	278	256	193	178	132
Meas. Dose [Gy]	211	198	192	183	164
Difference [%]	-24	-23	-1	3	24

instance, of $\sim 10 \times 10$ cm^2 with $\sigma = \pm 10\%$ and flux up to 5×10^5 HEH/cm^2/s.

Moreover, Table II summarizes the integral neutron flux above 10 and 20 meV, ThNeq and total flux, considering the surface covered by the Alliance memory (analogous values apply for the other SRAMs). As can be seen, a considerable fraction of neutrons has energy below 10 meV; hence, it is fundamental to consider the response function of each memory through the HEHeq fluence approach.

The measured SEEs are shown in Fig. 12 for the four SRAMs, in comparison to the events calculated through (4) by using the simulated spectrum (N4) of Fig. 4 and the response function of each memory from Fig. 2 to calculate the fluences (Φ_{HEHeq} and Φ_{ThNeq}). The SEE values are normalized to the memory size (Mbit) to have the same metric. The thermal neutron flux (Φ_{ThNeq}/t) used in (4) was calculated from (1) and is reported in Table II. The calculated SEEs are within 15% of the measured values for the Cypress and Alliance memories and 60% for the ISSI and Samsung memories. Considering the experimental and simulation uncertainties on the fluences ($\sim$30%), the agreement is satisfactory and proves the validity of the approach. Note that although the simulated HEH flux (see Fig. 11) is very similar in the positions of the Alliance and Samsung memories, the measured (and calculated) SEL count of Alliance is lower because of its higher E_{th}. Hence, with the Alliance and Samsung SEL memories, we are able to measure just a portion of the neutron spectrum, above $\sim$25 and $\sim$40 meV, respectively. Differently, with the ISSI and Cypress SEU memories, also neutrons with lower energies can be measured, and this is the reason why they measured higher SEE rates.

B. RPL Measurements and Benchmark With Simulations

The RPL dosimeters were installed in the same positions as the SRAMs in a separate run (see Fig. 11) and an additional RPL was placed in the center of the projection of the collimator on the wall (coordinates [0, 0] in the same figure). A dedicated simulation was run to score the dose in the RPLs, whose geometry and material were modeled in FLUKA. Table III reports the simulated and measured doses on these positions for a total of 8.4×10^{18} POT, where the initial letter of the SRAMs is used to identify the RPL position. As can be seen, the agreement is very good with a maximum difference of 24% between the measured dose with respect to the simulated value. Given the low dose values (achieved in about three months of irradiation), the N4 test position is not well-suited for total ionizing dose (TID) testing, but as mentioned before, this is good for SEEs. Only in N1, dose values up to 200 Gy can be achieved within one week of irradiation, similar to the dose rate of R1 at CHARM (see Fig. 9).

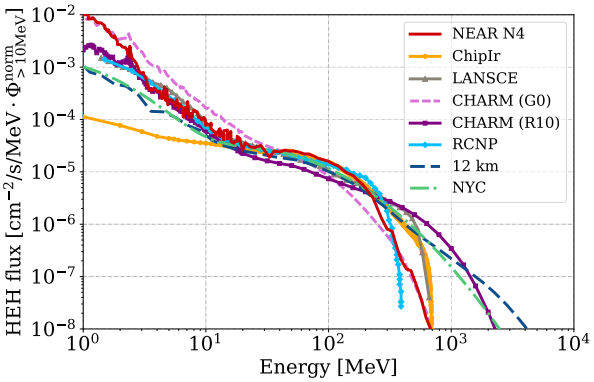

Fig. 13. Comparison of the n_TOF (NEAR) neutron spectrum to that of several spallation facilities, ground, and avionic environments, normalized so that the integral above 10 meV of each curve is the same. Notice that the spectra at CHARM above 20 meV include also other hadrons in addition to neutrons.

TABLE IV

HARDNESS FACTORS $H_{10\%}$ IN MEV OF SEVERAL ENVIRONMENTS CHARACTERIZED BY NEUTRONS. LARGER VALUES OF THIS FACTOR DENOTE SPECTRA WITH LARGER FLUXES AT HIGH ENERGIES

Env.	NEAR	LANSCE	RCNP	ChipIr	NYC	LHC (UJ)	CHARM (G0)
$H^{[MeV]}_{10\%}$	276	354	223	283	475	183	194

VI. COMPARISON WITH OTHER ENVIRONMENTS

The NEAR differential spectrum at n_TOF in position N4 is compared to other neutron environments in Fig. 13, normalized to the integral above 10 meV of the New York City (NYC) ground-level neutron spectrum (from the JESD89A [1] standard). ChipIr, LANSCE, and the RCNP [33] are spallation facilities providing atmospheric-like neutron spectra, and the avionic spectrum at 12 km of altitude is added for completeness from [21]. As can be seen, the NEAR spectrum is very similar to that at RCNP and compatible with the typical shape of spallation sources, hence, it is adequate for electronics testing.

To further compare the NEAR spectrum to other environments, such as those in the LHC, the hardness factor $H_{10\%}$ is defined as the energy above which 10% of the HEH flux (>20 meV) is still present in the spectrum of interest. The larger this value for a certain spectrum, the larger the flux at high energy. Table IV shows $H_{10\%}$ at NEAR compared to that of the facilities previously presented and accelerator environments: an actual LHC alcove hosting electronics (UJ) and a test position at CHARM characterized by a soft spectrum G0. NEAR, with an $H_{10\%}$ of 276 meV, is quite similar to RCNP, ChipIr, UJ, and G0, hence, it can be employed to mimic atmospheric or accelerator environments presenting a soft spectrum (hard spectra in the LHC can show hardness larger than 700 meV and this hardness can be achieved only at CHARM).

VII. CONCLUSION

The neutron field at the NEAR station of the n_TOF spallation source at CERN was characterized through Monte Carlo simulations, well-known SRAM devices, and RPL dosimeters. The study of the NEAR neutron environment had the aim of exploiting the potential of n_TOF for irradiation of electronics, as the availability of spallation sources in the world is limited.

An extensive Monte Carlo simulation analysis was carried out to study the radiation field of several test positions facing the main axis of the collimator and on the sides. In addition, the quantities relevant to the irradiation of electronics at NEAR were compared to those at CHARM, which is the reference facility for component and system qualification at CERN. The HEH flux (>20 meV), which is composed of neutrons at NEAR (>97%), can range from 10^9 to 10^{10} cm^{-2}/h in front of the collimator, and these values are compatible with the HEH fluxes at CHARM. Moreover, unlike the mixed-field at CHARM, the spectra at NEAR are composed of more than 99.7% of neutrons, which enables testing with a pure neutron field with energies from thermals up to ~830 meV. The test positions at NEAR with respect to those at CHARM present lower dose/HEH ratios and generally lower thermal neutron fluxes.

To validate the simulations, measurements with calibrated SRAMs and RPL dosimeters were carried out at a specific location on the wall in front of the collimator and a dedicated FLUKA analysis was here performed, by assessing the homogeneity of the beam. The approach of using SEU and SEL SRAMs, which are sensitive to different fractions of the wide neutron spectrum, permitted quantifying the neutron fluence through the SEE counts, yielding a satisfactory agreement with the simulations. The dose values were also validated by means of RPLs, resulting in agreement within 24% with the simulations. However, only the position immediately outside the collimator at NEAR (N1) can deliver a considerable dose in a relatively short time frame for TID qualification (200 Gy in about one week).

In conclusion, this work showed the potential of NEAR for the irradiation of electronics with a pure neutron spectrum, especially for SEE testing, for atmospheric and soft-spectra accelerator applications. Furthermore, the NEAR spectrum showed to be compatible with that of typical spallation sources for electronics qualification. It is worth noting that although CHARM was conceived and is operated as a user facility for electronic components and system qualification, n_TOF NEAR currently does not provide the service as a user facility and should therefore rather be considered as an experimental area for potential research and development applications, profiting from its specific radiation environment characteristics.

REFERENCES

[1] *Measurement and Reporting of Alpha Particle and Terrestrial Cosmic Ray-Induced Soft Errors in Semiconductor Devices*, JEDEC Standard JESD89A, Oct. 2006.

[2] ISO Central Secretary. *Process Management for Avionics-Atmospheric Radiation Effects, Accommodation of Atmospheric Radiation Effects Via Single Event Effects Within Avionics Electronic Equipment*, International Electrotechnical Commission, Geneva, CH, Standard IEC Standard 62396-1, 2017.

[3] ISO Central Secretary, *Process Management for Avionics-Atmospheric Radiation Effects, Guidelines for Single Event Effects Testing for Avionics Systems*, International Electrotechnical Commission, Geneva, CH, Standard IEC 62396-2, 2016.

[4] M. Cecchetto et al., "SEE flux and spectral hardness calibration of neutron spallation and mixed-field facilities," *IEEE Trans. Nucl. Sci.*, vol. 66, no. 7, pp. 1532–1540, Jul. 2019.

[5] J. Mekki et al., "CHARM: A mixed field facility at CERN for radiation tests in ground, atmospheric, space and accelerator representative environments," *IEEE Trans. Nucl. Sci.*, vol. 63, no. 4, pp. 2106–2114, Aug. 2016.

[6] C. Cazzaniga and C. D. Frost, "Progress of the scientific commissioning of a fast neutron beamline for chip irradiation," *J. Phys., Conf.*, vol. 1021, May 2018, Art. no. 012037.

[7] *n_TOF*. Accessed: Apr. 1, 2022. [Online]. Available: https://www.cernch/ntof

[8] V. Vlachoudis, "FLAIR: A powerful but user friendly graphical interface for FLUKA," in *Proc. Int. Conf. Math., Comput. Methods React. Phys. (MC)*, Saratoga Springs, NY, USA, 2009, pp. 790–800.

[9] G. Battistoni et al., "Overview of the FLUKA code," *Ann. Nucl. Energy*, vol. 82, pp. 10–18, Aug. 2015.

[10] C. Ahdida et al., "New capabilities of the FLUKA multi-purpose code," *Frontiers Phys.*, vol. 9, p. 705, Jan. 2022.

[11] M. Cecchetto et al., "0.1–10 MeV neutron soft error rate in accelerator and atmospheric environments," *IEEE Trans. Nucl. Sci.*, vol. 68, no. 5, pp. 873–883, May 2021.

[12] D. Pramberger, Y. Q. Aguiar, J. Trummer, and H. Vincke, "Characterization of radio-photo-luminescence (RPL) dosimeters as radiation monitors in the CERN accelerator complex," *IEEE Trans. Nucl. Sci.*, vol. 69, no. 7, pp. 1618–1624, Jul. 2022.

[13] C. Guerrero et al., "Performance of the neutron time-of-flight facility n_TOF at CERN," *Eur. Phys. J. A*, vol. 49, no. 2, pp. 1–15, Feb. 2013.

[14] N. Colonna, F. Gunsing, and E. Chiaveri, "The second beam-line and experimental area at n_TOF: A new opportunity for challenging neutron measurements at CERN," *Nucl. Phys. News*, vol. 25, no. 4, pp. 19–23, Dec. 2015.

[15] C. Borcea et al., "Results from the commissioning of the n_TOF spallation neutron source at CERN," *Nucl. Instrum. Methods Phys. Res. Sect. A*, vol. 513, no. 3, pp. 524–537, Nov. 2003.

[16] C. Rubbia et al., "A high resolution spallation driven facility at the CERN-PS to measure neutron cross sections in the interval from 1 eV to 250 MeV: A relative performance assessment," CERN, Geneva, Switzerland, Tech. Rep., CERN-LHC-98-002-EET-Add.1, 1998, Accessed: Aug. 2022. [Online]. Available: https://cds.cern.ch/record/363828

[17] R. Esposito and M. Calviani, "Design of the third-generation neutron spallation target for the CERN's n_TOF facility," *J. Neutron Res.*, vol. 22, nos. 2–3, pp. 221–231, Oct. 2020.

[18] R. Esposito et al., "Design of the third-generation lead-based neutron spallation target for the neutron time-of-flight facility at CERN," *Phys. Rev. A, Gen. Phys.*, vol. 24, no. 9, Sep. 2021, Art. no. 093001.

[19] M. Ferrari et al., "Design development and implementation of an irradiation station at the neutron time-of-flight facility at CERN," *Phys. Rev. A, Gen. Phys.*, vol. 25, no. 10, Oct. 2022, Art. no. 103001.

[20] R. G. Alía et al., "SEL hardness assurance in a mixed radiation field," *IEEE Trans. Nucl. Sci.*, vol. 62, no. 6, pp. 2555–2562, Dec. 2015.

[21] M. Cecchetto, R. García Alía, and F. Wrobel, "Impact of energy dependence on ground level and avionic SEE rate prediction when applying standard test procedures," *Aerospace*, vol. 6, no. 11, p. 119, Nov. 2019.

[22] R. G. Alía et al., "SEL cross section energy dependence impact on the high energy accelerator failure rate," *IEEE Trans. Nucl. Sci.*, vol. 61, no. 6, pp. 2936–2944, Oct. 2014.

[23] M. Cecchetto et al., "Thermal neutron-induced SEUs in the LHC accelerator environment," *IEEE Trans. Nucl. Sci.*, vol. 67, no. 7, pp. 1412–1420, Jul. 2020.

[24] A. Coronetti et al., "Assessment of proton direct ionization for the radiation hardness assurance of deep submicron SRAMs used in space applications," *IEEE Trans. Nucl. Sci.*, vol. 68, no. 5, pp. 937–948, May 2021.

[25] G. Lerner et al., "Analysis of the radiation field generated by 200-MeV electrons on a target at the CLEAR accelerator at CERN," *IEEE Trans. Nucl. Sci.*, Feb. 2023.

[26] M. Cecchetto, R. G. Alía, S. Gerardin, M. Brugger, A. Infantino, and S. Danzeca, "Impact of thermal and intermediate energy neutrons on SRAM SEE rates in the LHC accelerator," *IEEE Trans. Nucl. Sci.*, vol. 65, no. 8, pp. 1800–1806, Aug. 2018.

[27] K. Roeed et al., "Method for measuring mixed field radiation levels relevant for SEEs at the LHC," *IEEE Trans. Nucl. Sci.*, vol. 59, no. 4, pp. 1040–1047, Aug. 2012.

[28] J. Beaucour et al., "Grenoble large scale facilities for advanced characterisation of microelectronics devices," in *Proc. 15th Eur. Conf. Radiat. Effects Compon. Syst. (RADECS)*, Moscow, Russia, Sep. 2015, pp. 312–315.

[29] R. G. Alía et al., "Energy dependence of tungsten-dominated SEL cross sections," *IEEE Trans. Nucl. Sci.*, vol. 61, no. 5, pp. 2718–2726, Oct. 2014.

[30] *FLUKA Manual*. Accessed: Jun. 1, 2022. [Online]. Available: https://flukafiles.web.cern.ch/manual/index.html

[31] R. G. Alia et al., "LHC and HL-LHC: Present and future radiation environment in the high-luminosity collision points and RHA implications," *IEEE Trans. Nucl. Sci.*, vol. 65, no. 1, pp. 448–456, Jan. 2018.

[32] A. Coronetti et al., "The pion single-event effect resonance and its impact in an accelerator environment," *IEEE Trans. Nucl. Sci.*, vol. 67, no. 7, pp. 1606–1613, Jul. 2020.

[33] Y. Iwamoto et al., "Evaluation of the white neutron beam spectrum for single-event effects testing at the RCNP cyclotron facility," *Nucl. Technol.*, vol. 173, no. 2, pp. 210–217, Apr. 2017.